Characterisation and structure analysis of taxanes-loaded human serum albumin nanoparticles prepared by self-assembly method

Ru Fang, Yanbin Wang, Bentong Liu, Hua Qian, Shaozong Yang ✉

Institute of Forest Food, Zhejiang Academy of Forestry, Hangzhou 310023, People's Republic of China
✉ *E-mail: yangsz863@163.com*

Published in Micro & Nano Letters; Received on 28th February 2018; Revised on 28th March 2018; Accepted on 9th April 2018

In this work, human serum albumin (HSA) was used to prepare core-shell taxanes-loaded nanoparticle (NP) by self-assembly method. Various experimental technologies were used to character two different taxanes-loaded HSA NPs and analyse the structure of them. The obtained NPs had a spherical morphology and core-shell structure. The data revealed that one paclitaxel (PTX)-loaded HSA NP (~40 nm) consisted of six HSA molecules and 34 PTX molecules, and one docetaxel (DOC)-loaded HSA NP (~30 nm) consisted of five HSA molecules and 40 DOC molecules. The infrared, three-dimensional fluorescence and ultraviolet absorption spectra showed that intermolecular hydrogen bond occurred between taxanes and polypeptide chain of HSA and resulted in change of its secondary structure. The fluorescence spectra experiment results suggested that PTX and DOC interacted with tryptophan (Trp)-214, which lie on site I of HSA, and the type of interactions were hydrogen bond and hydrophobic interaction, respectively. It suggested that the binding mode of taxanes with Trp-214 is the primary factor that determined the size and loading capacity of taxanes-loaded HSA NPs. This work indicates that such HSA NP is very promising in the field of nanoscale drug delivery systems research.

1. Introduction: To avoid the problems caused by adjuvants, commonly approaches to improve the aqueous solubility of hydrophobic drugs, various nanoscale drug delivery systems (DDSs) were currently investigated. Recently, the protein-based nanoscale platform aroused more attention due to their biocompatibility and biodegradability coupled with low toxicity. Various protein-based nanoscale platforms have been investigated including protein cage, hydrogel, film, nanoparticle (NP), minirod and minipellet. Among them, protein NP has drawn much attention because of its stability during storage and ease to control during manufacture. Nowadays various researches have touched the preparation of NPs using proteins like gelatin, lipoprotein, albumin, gliadin and legumin.

Albumins, being commonly found in blood plasma, are attractive natural proteins and can transport various endogenous or exogenous compounds throughout the body. It was confirmed that albumin promoted endothelial transcytosis of various drugs, which was subsequently transported to the extracellular space through binding to glycoprotein (gp60) receptor [1–3]. secreted protein, acidic and rich in cysteine, which is believed to be selectively secreted by tumours (e.g. breast, lung, and prostate), binds albumin and facilitates the intratumour accumulation of albumin bound drugs [4, 5]. So, albumin based NP is particularly interesting as DDS of anticarcinogen. Commercially, albumins are obtained from egg white (ovalbumin), bovine serum (bovine serum albumin, BSA) and human serum (human serum albumin, HSA). BSA and HSA were both utilised to prepare NPs as DDS, and the most successful was HSA NP carrier developed by nab-technology. As an HSA NP-based paclitaxel (PTX) formulation, Abraxaner® is the only nanoscale DDS PTX formulation approved by both Food and Drug Administration (FDA) and European Medicines Evaluation Agency (EMEA) for use in treating cancers [6, 7].

The main objective of this study was to develop a core-shell HSA NP as delivery system by self-assembly method. The core-shell structural NP gained traction because of its structure and composition flexibility. The hydrophilic shell serves as a stabilising interface of NP and can protect drug from binding to blood proteins and being absorbed into the reticuloendothelial system, thus keeping drug in the systemic circulation for a prolonged period of time [8–10]. The hydrophobic core serves as the container of hydrophobic drug. The core-shell polymeric NP can increase the intracellular concentration of drug in malignant cells through endocytic pathways, overcome P-glycoprotein-mediated multidrug resistance (MDR) and protect drug from MDR-accelerated efflux [11, 12].

Taxanes, in particular PTX and docetaxel (DOC), had been considered by the National Cancer Institute as the most significant advance in drug discovery for chemotherapy and had become the most successful commercially antineoplastic agent [13, 14]. In this Letter, the core-shell HSA NP will be used to encapsulate taxanes. Moreover, we will characterise the size, morphology and structure of PTX-loaded HSA NP (PTX-HSANP) and DOC-loaded HSA NP (DOC-HSANP), and analyse the changes of chemical structure and molecular environment of HSA with the encapsulating of PTX or DOC.

2. Experimental: HSA (A-1653) and dimethyl sulfoxide (DMSO) were purchased from Sigma-Aldrich (MO, USA). PTX and DOC (purity > 98.0%) were purchased from Nanjing Zelang Biology Technology Co. Ltd. (Nanjing, China). The stock solutions (1.5×10^{-3} mol·L^{-1}) of HSA and taxanes were prepared with Milli-Q water (18.2 MΩ, Millipore Corp., MA, USA) and DMSO, respectively.

The various aqueous dispersions of taxanes-loaded HSA NP were prepared as below: Milli-Q water was added in the HSA stock solutions and stirred at 500 rpm, and then the taxanes stock solution and DMSO were added in the solution. In the final system, the concentrations of HSA and DMSO were 1.5×10^{-5} mol·L^{-1} and 30% (v/v), respectively, and the concentration of taxanes was adjusted from 1.5×10^{-5} to 1.5×10^{-4} mol·L^{-1}. The self-assembly taxanes-loaded HSA NP powders were obtained via the homologous procedure with the assistance of lyophilisation technology: Milli-Q water was added in the HSA stock solutions, and then the taxanes stock solution and DMSO were added in the solution. In the final system, the concentrations of HSA, taxane and DMSO were 1.5×10^{-5} mol·L^{-1}, 1.5×10^{-4} mol·L^{-1} and 30% (v/v), respectively. Subsequently, the solution was freeze-dried to remove DMSO and obtain dry powders, which contain HSA NPs entrapping taxanes and free taxanes that were not entrapped. Milli-Q water was added in the powders, and then the redissolved solution was centrifuged under at 15,000 rpm for

© The Institution of Engineering and Technology 2018

20 min. The precipitate was removed and supernatant was freeze-dried again to obtain self-assembly taxanes-loaded HSA NP powders.

Scanning transmission electron microscopy (STEM), dynamic light scattering (DLS), static light scattering (SLS), Raman spectroscopy, Fourier transform infrared spectrometer (FTIR), fluorescence spectrometry and UV–vis absorption spectrometry were applied to characterise the morphology and structure of the NPs. The taxanes-binding capacity of NPs was determined using isocratic reversed-phase high-performance liquid chromatography (HPLC) with UV detector at 228 nm.

3. Results and discussion: STEM and DLS were combined to investigate the morphology and size of the taxanes-loaded HSA NPs. As shown in the STEM micrographs (Fig. 1), the NPs displayed compact and spherical aggregates with size <50 nm. From the results of DLS, the average hydrodynamic particle size of PTX-HSANPs was larger than DOC-HSANPs (38.51 ± 5.91 nm versus 26.37 ± 3.58 nm). There was no significant difference of the zeta potential value of between PTX-HSANPs and DOC-HSANPs ($P > 0.05$), and it was about −30 mV.

The average molecular mass of taxanes-loaded HSA NP was determined using SLS method, and the Mw of PTX-loaded HSA NP and DOC-loaded HSA NP were 440.92 ± 37.46 and 362.23 ± 13.28 kDa, respectively. The amount of taxanes in the taxanes-loaded HSA NP was determined using HPLC method. It was found that the ratios of PTX/HSA and DOC/HSA in the NP were 5.5 and 8.2, respectively. In summary, it means that one PTX-loaded HSA NP consisted of six HSA molecules and 34 PTX molecules, and one DOC-loaded HSA NP consisted of five HSA molecules and 40 DOC molecules.

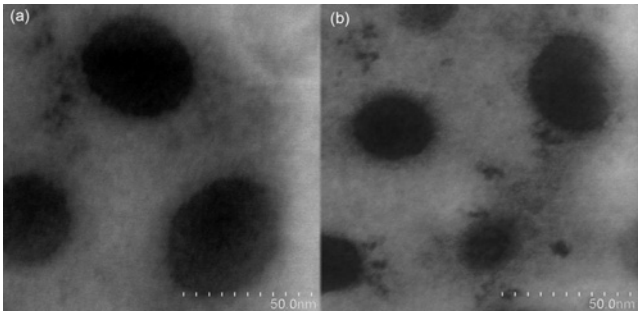


Fig. 1 *STEM images of different NPs*
a PTX-HSANP
b DOC-HSANP

The three-dimensional fluorescence spectra of HSA (a), PTX-HSANP (b) and DOC-HSANP (c) systems are shown in Fig. 2. Peak 1 mainly reveals the spectral feature of the polarity of tryptophan (Trp) and tyrosine (Tyr) residues microenvironment [15]. Peak 2 chiefly exhibits the fluorescence spectrum behaviour of polypeptide chain backbone structures, which results from n–π^* electronic transitions of C=O groups. As shown in Table 1, the fluorescence intensity of peak 2 was completely disappeared in the PTX-HSANP system and almost disappeared in the DOC-HSANP system, which implied the conformational change of the peptide backbone resulted from the degeneracy of n–π^* states [16, 17].

Fig. 3 shows the FTIR spectra of HSA (a), PTX-HSANP (b) and DOC-HSANP (c) systems. The protein secondary structure can be determined from the shape of the amide I and amide II band. The amide I band (1700–1600 cm^{-1}) is due almost entirely to the C=O stretch vibrations of the peptide linkages (~80%). The amide II band (1600–1490 cm^{-1}) derives mainly from in-plane NH bending (40–60% of the potential energy) and from the CN stretching vibration (18–40%) [17, 18]. The IR peaks at 1653 and 1536 cm^{-1} were assigned to amides I and II band of HSA, respectively. A bathochromic shift of amide I band (from 1653 to 1655 cm^{-1}) and amide II band (from 1536 to 1541 cm^{-1}) was observed in the cases of PTX-HSANP and DOC-HSANP. The observed frequency variations of such bands indicated a decrease of the transition energy, which resulted from the combination of taxanes and the peptide backbone C=O stretch, stretching vibrations δ_{NH} and υ_{C-N} of HSA through hydrogen bond. The intermolecular hydrogen bond destroyed the peptide backbone of HSA [19].

The UV–vis absorption spectrum of taxanes at 200–300 nm has one band, which is associated with their chromophoric group. As shown in Fig. 4, the characteristic band of PTX and DOC was at 233 and 234 nm (solid line), respectively. However, a red shift of 4 and 3 nm of the band was observed in the case of HSA NP encapsulated PTX and DOC (dot line). As reported, the lone-pair electrons in the auxochromic group will conjugate with the chromophoric group when the hydrogen bonding has occurred between them. This leads to a decrease of the π–π^* transition energy with the bathochromic shift UV–vis [20, 21]. It could be concluded that a hydrogen bond formed between PTX or DOC and HSA. This was consistent with the analysis of FTIR spectra, it referred that PTX or DOC interacted with the peptide backbone C=O stretch, stretching vibrations δ_{NH} and υ_{C-N} of HSA through hydrogen bond.

As reported in some studies, DMSO resulted in the partial unfolding of the polypeptide chain through hydrogen bonding

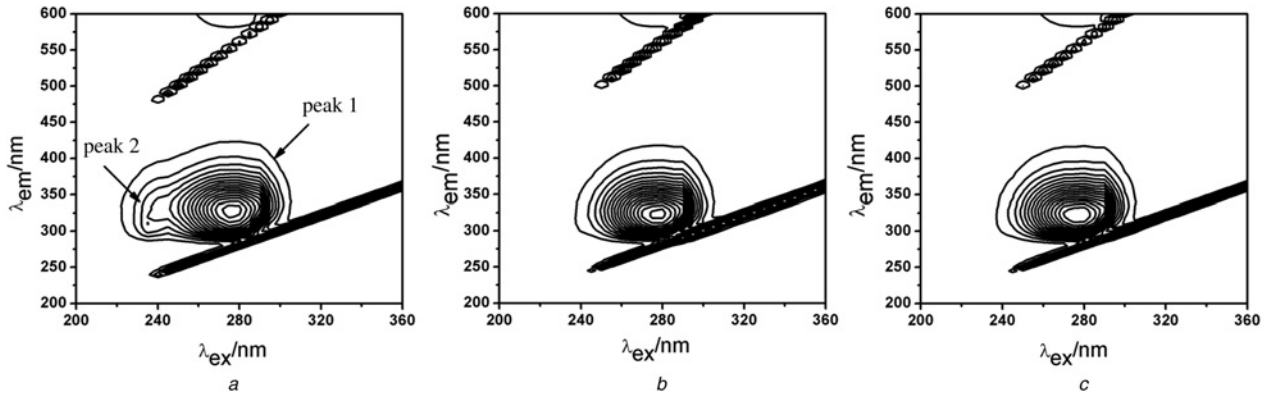


Fig. 2 *Contour fluorescence spectra of different systems*
a HSA
b PTX-HSANP
c DOC-HSANP

© The Institution of Engineering and Technology 2018

doi: 10.1049/mnl.2018.0165

interaction between the S=O group of DMSO and the C=O stretch of HSA. Meanwhile, taxanes (PTX or DOC) also promoted the changes of the secondary structure of HSA. As a result, the molecular rearrangement of HSA occurred and contributed to the formation of the taxanes-loaded HSA NPs.

Fig. 5 shows the quenching effect of PTX (a) and DOC (b) on the fluorescence emission spectra of HSA. The fluorescence intensity of HSA decreased regularly with increasing PTX or DOC concentration. After the addition of DOC, the peak of HSA had a blue shift (from 325 to 320 nm). This indicated that the microenvironment of Trp or Tyr residue was more hydrophobic. It is noteworthy that no detectable shift was observed with addition of PTX.

Quenching processes usually involve two modes, dynamic and static. To elucidate the type of fluorescence quenching mode, the fluorescence quenching data were analysed with the Stern–Volmer (1) [22, 23]:

$$\frac{F_0}{F} = 1 + K_q \tau_0 [Q] = 1 + K_{SV}[Q] \quad (1)$$

Table 1 Three-dimensional fluorescence spectral characteristic parameters of different systems

	HSA		PTX-HSANP		DOC-HSANP	
	Peak 1	Peak 2	Peak 1	Peak 2	Peak 1	Peak 2
peak position $\lambda_{ex}/\lambda_{em}$, nm/nm	275/325	235/310	280/325		280/320	205/320
intensity F	594.82	125.83	560.56		577.74	4.02

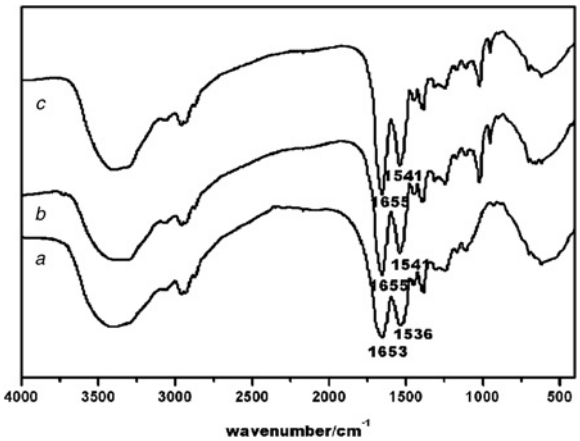


Fig. 3 *FTIR spectra of different systems*
a HSA
b PTX-HSANP
c DOC-HSANP

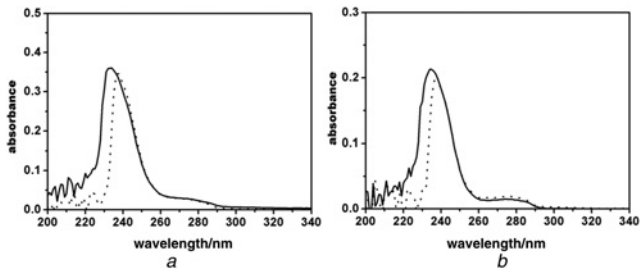


Fig. 4 *UV–vis absorption of the taxanes (solid) and the encapsulated taxanes (dot)*
a PTX-HSANP
b DOC-HSANP

where F_0 and F represent the fluorescence intensities without and with taxanes, respectively. $[Q]$ is the concentration of taxanes. K_q is the quenching rate constant and τ_0 is the phosphorescence lifetime in the absence of taxanes. K_{SV} is defined as Stern–Volmer quenching constant.

Fig. 6 shows the Stern–Volmer plots of the quenching of HSA by PTX and DOC at different temperatures. A good relationship between points and the calculated values was observed. Based on the experimental data, the corresponding calculated dynamic quenching constants for the interaction between taxanes and HSA are shown in Table 2. For dynamic quenching, the maximum K_q of various quenchers with the biomacromolecule is about 2.0×10^{10} L·mol^{-1}·s^{-1} [24]. The K_q of HSA quenching procedure initiated by PTX or DOC is much $>2.0 \times 10^{10}$ L·mol^{-1}·s^{-1}. It can be concluded that the quenching is not initiated by dynamic quenching, but probably by static quenching resulting from the formation of HSA-PTX or HSA-DOC complexes. As shown in Table 2, the K_{SV} decreased with increased temperatures in the system of PTX-HSANP and increased with increased temperatures in the system of DOC-HSANP.

For static quenching, the relationship between fluorescence quenching intensity and the concentration of quenchers can be described as [25, 26]

$$\lg\left[\frac{(F_0 - F)}{F}\right] = \lg K_\alpha + n \lg [Q] \quad (2)$$

where K_α is the binding constant, and n is the number of binding sites per HSA molecular. Based on the fluorescence quenching

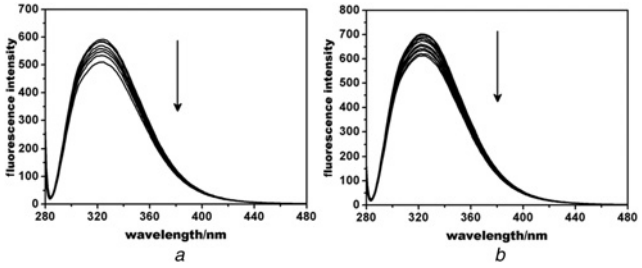


Fig. 5 *Fluorescence quenching spectra of different systems*
a PTX-HSANP
b DOC-HSANP

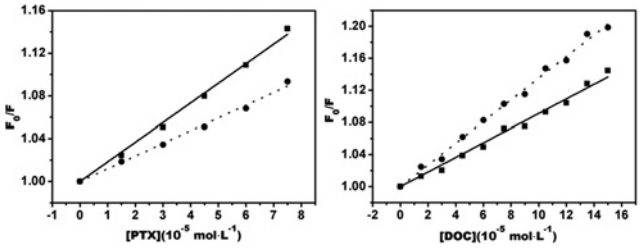


Fig. 6 *Stern–Volmer plots of fluorescence quenching of different systems at different temperatures (filled square 300 K, filed circle 310 K)*

Table 2 Quenching constants of different systems at different temperatures

System	T/K	K_{SV}, L·mol^{-1}	K_q, L·mol^{-1}·s^{-1}	R
PTX-HSANP	300	0.18×10^4	0.18×10^{12}	0.999
	310	0.12×10^4	0.12×10^{12}	0.999
DOC-HSANP	300	0.09×10^4	0.09×10^{12}	0.999
	310	0.14×10^4	0.14×10^{12}	0.999

© The Institution of Engineering and Technology 2018

intensities in Fig. 5, the double-logarithm algorithm was assessed in (2). Fig. 7 shows the double-logarithm curves, and Table 3 presents the corresponding calculated results. The linear correlation coefficients for the curves are >0.990, indicating that the interaction between taxanes and HSA agrees well with the site-binding model underlying (2). The result illustrates that there is a strong binding force between taxanes and HSA, and that one binding site would be formed [25–27].

In order to elucidate the interaction (hydrophobic force, electrostatic interaction, van der Waals interaction or hydrogen bond) of taxanes with HSA, we calculated the thermodynamic parameters as follows [28]:

$$\ln\left(\frac{K_{\alpha 2}}{K_{\alpha 1}}\right) = -\frac{\Delta H}{R}\left(\frac{1}{T_2} - \frac{1}{T_1}\right) \tag{3}$$

where R (8.314 J·mol^{-1}·K^{-1}) is the gas constant, T (K) is the experimental temperature. Then, ΔH and entropy change (ΔS, J·mol^{-1}·K^{-1}) can be calculated from the following equations [28, 29]:

$$\Delta G = -RT \ln K \tag{4}$$

$$\Delta G = \Delta H - T\Delta S \tag{5}$$

The thermodynamic parameters for the interaction of PTX or DOC with HSA are shown in Table 4, there are some different calculations between PTX and DOC. The negative sign for ΔG means that the interaction process is spontaneous. The negative ΔH and ΔS values indicate that the binding between PTX and HSA is mainly ΔH driven, with little contribution from the entropy factor, and hydrogen bond may play a major role in the reaction. The positive ΔH and ΔS values indicate that the binding between DOC and HSA is mainly ΔS driven, with little contribution from the enthalpy factor, and hydrophobic force may play a major role in the reaction [30].

The synchronous fluorescence spectra can provide information of the molecular environment in the vicinity of the chromosphere molecules. Fig. 8 shows the effect of PTX (a and b) and DOC (c and d) on the synchronous fluorescence of the Tyr ($\Delta\lambda = 15$ nm) and Trp ($\Delta\lambda = 60$ nm) in HSA. It was observed that both the fluorescence of Trp and Tyr residues were quenched by PTX and DOC. Fig. 9 shows the Stern–Volmer plots of synchronous fluorescence quenching of Tyr and Trp by PTX and DOC. It was observed that the fluorescence quenching of Trp was much bigger than that of Tyr, suggesting that the binding site for taxanes was located at Trp residue in HSA.

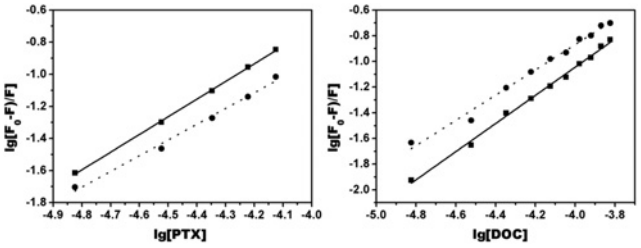


Fig. 7 *Double lg plots of fluorescence quenching of different systems at different temperatures (filled square 300 K, filed circle 310 K)*

Table 3 Binding parameters of different systems at different temperatures

System	T/K	K_α, L·mol^{-1}	n	R
PTX-HSANP	300	4.88×10^3	1.10076	0.999
	310	1.00×10^3	0.97997	0.991
DOC-HSANP	300	1.16×10^3	0.98353	0.990
	310	2.18×10^3	1.09587	0.996

Table 4 Thermodynamic parameters of different systems at different temperatures

System	T, K	ΔG, kJ·mol^{-1}	ΔH, kJ·mol^{-1}	ΔS, J·mol^{-1}·K^{-1}
PTX-HSANP	300	−21.18	−119.74	−328.50
	310	−17.81		
DOC-HSANP	300	−17.60	47.69	217.6
	310	−19.81		

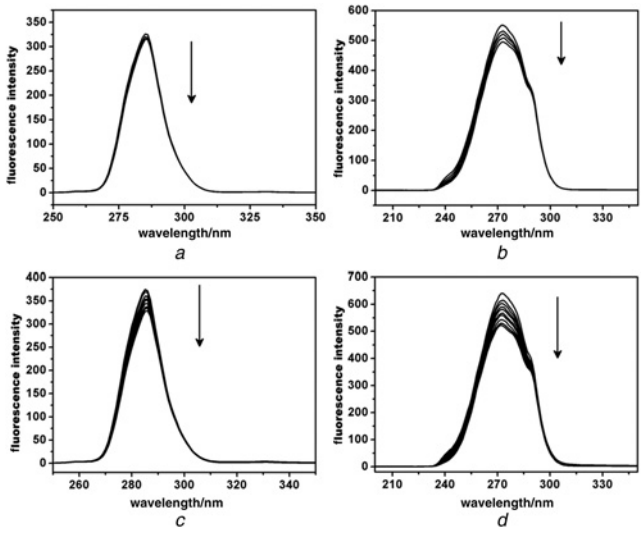


Fig. 8 *Synchronous fluorescence spectra of different systems*
a PTX-HSANP, $\Delta\lambda = 15$ nm
b PTX-HSANP, $\Delta\lambda = 60$ nm
c DOC-HSANP, $\Delta\lambda = 15$ nm
d DOC-HSANP, $\Delta\lambda = 60$ nm

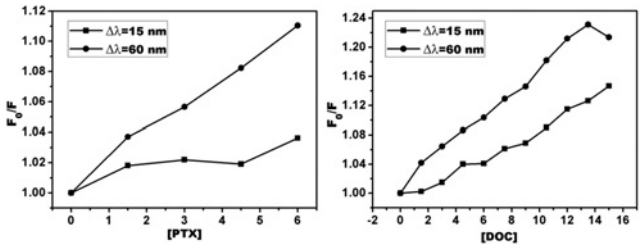


Fig. 9 *Comparison of synchronous fluorescence quenching of different systems*

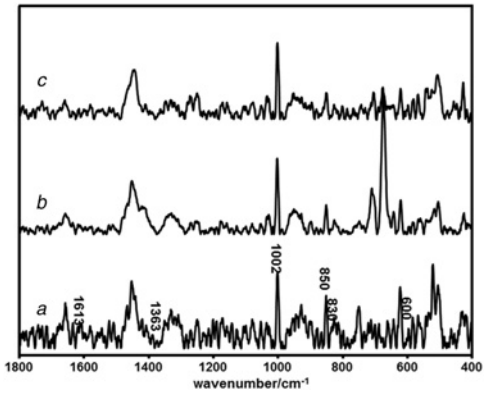


Fig. 10 *Raman spectra of different systems*
a HSA
b PTX-HSANP
c DOC-HSANP

© The Institution of Engineering and Technology 2018

doi: 10.1049/mnl.2018.0165

Table 5 Intensities[a] of Raman band of different systems

System	830 cm^{-1}	850 cm^{-1}	600 cm^{-1}	1613 cm^{-1}	1363 cm^{-1}
HSA	0.32	0.59	0.26	0.31	0.10
PTX-HSANP	0.19	0.39	0.10	0.12	0.06
DOC-HSANP	0.12	0.35	0.18	0.14	0.13

[a]Integrated intensity (peak intensity) relative to that of the phenylalanine band at 1002 cm^{-1}.

Raman spectra (1800–400 cm^{-1}) of native HSA and taxanes-loaded HSA are exhibited in Fig. 10. The integrated intensities for several peaks ascribing to side chains of Trp and Tyr are summarised in Table 5. The intensity ratio of the Tyr Fermi doublets (850/830 cm^{-1}) indicates that the state of phenolic hydroxyl group in Tyr, such as buried, exposed, hydrogen-bond acceptor or donor and ionic [31–33]. It can be seen from Table 5 that both the values of I_{850}/I_{830} for native HSA and taxanes-loaded HSA are >1.5, indicating that Tyr residues may not be involved in hydrogen bonding interaction between taxanes and HSA.

There are several vibration bands can provide information on the microenvironment of Trp residue side chains. The band near 600 cm^{-1} is ascribed to the pyrrole ring skeletal of Trp. The band at 1613 cm^{-1}, which is sensitive to the bound ligands, is a marker of the orientation of the indole ring of Trp with respect to the C_α atom of the peptide backbone [34, 35]. The varieties in band intensities shown in Table 5 indicate that the embedded taxanes lead to the reorientation of the pyrrole and indole ring through the adjustment in the torsional angle of the side chain. The band at 1363 cm^{-1} was found to be indicator of the hydrophobicity of the Trp environment [33]. The decrease in this band intensity for PTX-HSANP indicated that the molecular environment of Trp was less hydrophobic due to the hydrogen bonding interaction between the PTX and Trp. In contrast, the increase in this band intensity for DOC-HSANP indicated that the molecular environment of Trp was more hydrophobic. This was consistent with the analysis of fluorescence spectra.

Sites I and II had been proved to be the binding sites of HSA for various hydrophobic drugs. As confirmed in the fluorescence spectra analysis, there is just one binding site in HSA for PTX or DOC, and the binding site is nearby the Trp residue. There is only one Trp residue in HSA (Trp-214), which is located at Sudlow's site I. Thermodynamic data indicated that the interaction force between PTX and Trp-214 was different from that between DOC and Trp-214. It inferred that this difference was related to the structure of two taxanes. As shown in Fig. 11, there are two variations at C10 and C4′ in the structure of PTX and DOC. It was the C4′-carbonyl group that determined the type of interaction force between taxanes and HSA. The C4′-carbonyl group in PTX is adjacent to the aromatic hydrocarbon, and that in DOC is adjacent to the fatty hydrocarbon. As a result, the C4′-carbonyl group in PTX is more active than that in DOC, and can conjugate with the aromatic hydrocarbon to form electron-donating group. This leads to a hydrogen bond formed between the C4′-carbonyl group in PTX and the amino-group of Trp-214. While the C4′-carbonyl group in DOC interacted with Trp-214 through hydrophobic force instead of hydrogen bond.

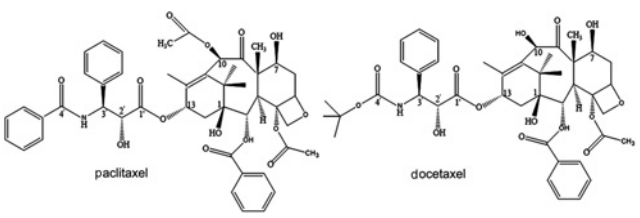


Fig. 11 *Structures of PTX and DOC*

4. Conclusion: In this Letter, an HSA NP was prepared by self-assembly method and used to encapsulate two taxanes, PTX and DOC. It exhibited that the taxanes-loaded HSA NP possessed a core-shell structure with sizes <50 nm. The formation mechanism of PTX-HSANP and DOC-HSANP was studied using various spectral methods and important results were obtained. With assistance of DMSO, taxanes resulted in the HSA molecules partially unfolded and aggregated to form core-shell NP by hydrophobic effects. Taxanes were embedded in the hydrophobic core of HSA NP and the binding site is located at site I near Trp-214. Interestingly, it was found that the interaction force between PTX and Trp-214 was different from the interaction force between DOC and Trp-214. The former was hydrogen bond and latter was hydrophobic force. The hydrogen bond formation between PTX and Trp-214 implied that the hydrophobicity of binding site decreased. Conversely, the hydrophobic force between DOC and Trp-214 increased the hydrophobicity of binding site. As a result, the hydrophobic core of DOC-HSANP was more compact than that of PTX-HSANP. This deduction is identical with the characterisation of two NPs. Despite the size of DOC-HSANP is smaller than that of PTX-HSANP (26.37 ± 3.58 nm versus 38.51 ± 5.91 nm), DOC-HSANP contain more taxanes than PTX-HSANP (40 DOC molecules versus 34 PTX molecules).

5. Acknowledgments: This study was supported by the Natural Science Foundation of Zhejiang Province (grant no. LQ15C160001) and Science and Technology Project of Zhejiang Province (grant no. 2014F30001).

6 References

[1] Houghton P.J., Kurmasheva R.T., Kolb E.A., *ET AL.*: 'Initial testing (stage 1) of the tubulin binding agent nanoparticle albumin-bound (nab) paclitaxel (Abraxane®) by the pediatric preclinical testing program (PPTP)', *Pediatr. Blood Cancer*, 2015, **62**, (7), pp. 1214–1221

[2] Mocan L., Matea C., Tabaran F.A., *ET AL.*: 'Photothermal treatment of liver cancer with albumin-conjugated gold nanoparticles initiates Golgi apparatus-ER dysfunction and caspase-3 apoptotic pathway activation by selective targeting of Gp60 receptor', *Int. J. Nanomed.*, 2015, **10**, p. 5435

[3] Zhao M., Lei C., Yang Y., *ET AL.*: 'Abraxane, the nanoparticle formulation of paclitaxel can induce drug resistance by up-regulation of P-gp', *PLoS One*, 2015, **10**, (7), p. e0131429

[4] Neesse A., Frese K.K., Chan D.S., *ET AL.*: 'SPARC independent drug delivery and antitumour effects of nab-paclitaxel in genetically engineered mice', *Gut*, 2014, **63**, (6), pp. 974–983

[5] Wagner L.M., Yin H., Eaves D., *ET AL.*: 'Preclinical evaluation of nanoparticle albumin-bound paclitaxel for treatment of pediatric bone sarcoma', *Pediatr. Blood Cancer*, 2014, **61**, (11), pp. 2096–2098

[6] Miele E., Spinelli G.P., Miele E., *ET AL.*: 'Albumin-bound formulation of paclitaxel (Abraxane® ABI-007) in the treatment of breast cancer', *Int. J. Nanomed.*, 2009, **4**, p. 99–105

[7] Vishnu P., Roy V.: 'Safety and efficacy of nab-paclitaxel in the treatment of patients with breast cancer', *Breast Cancer-Tokyo*, 2011, **5**, pp. BCBCR–S5857

© The Institution of Engineering and Technology 2018

[8] Sahoo S.K., Labhasetwar V.: 'Enhanced antiproliferative activity of transferrin-conjugated paclitaxel-loaded nanoparticles is mediated via sustained intracellular drug retention', *Mol. Pharmace*, 2005, **2**, (5), pp. 373–383
[9] Li W., Peng H., Ning F., *ET AL.*: 'Amphiphilic chitosan derivative-based core–shell micelles: synthesis, characterisation and properties for sustained release of vitamin D3', *Food Chem.*, 2014, **152**, pp. 307–315
[10] Danafar H., Davaran S., Rostamizadeh K., *ET AL.*: 'Biodegradable m-PEG/PCL core-shell micelles: preparation and characterization as a sustained release formulation for curcumin', *Adv. Pharm. Bull.*, 2014, **4**, (Suppl. 2), p. 501
[11] Némati F., Dubernet C., Fessi H., *ET AL.*: 'Reversion of multidrug resistance using nanoparticles in vitro: influence of the nature of the polymer', *Int. J. Pharm.*, 1996, **138**, (2), pp. 237–246
[12] Fang C., Zhang M.: 'Nanoparticle-based theragnostics: integrating diagnostic and therapeutic potentials in nanomedicine', *J. Control. Release*, 2010, **146**, (1), p. 2
[13] Wani M.C., Taylor H.L., Wall M.E., *ET AL.*: 'Plant antitumor agents. VI. Isolation and structure of taxol, a novel antileukemic and antitumor agent from Taxus brevifolia', *J. Am. Chem. Soc.*, 1971, **93**, (9), pp. 2325–2327
[14] Schiff P.B., Fant J., Horwitz S.B.: 'Promotion of microtubule assembly in vitro by taxol', *Nature*, 1979, **277**, (5698), p. 665
[15] Sun H., Wu Y., Xia X., *ET AL.*: 'Spectroscopic studies on the interaction characteristics between norethisterone and bovine serum albumin', *J. Lumin.*, 2013, **134**, pp. 580–587
[16] Kandagal P.B., Ashoka S., Seetharamappa J., *ET AL.*: 'Study of the interaction of an anticancer drug with human and bovine serum albumin: spectroscopic approach', *J. Pharmaceut. Biomed.*, 2006, **41**, (2), pp. 393–399
[17] Kong L., Hu J., Qin D., *ET AL.*: 'Interaction of ifosfamide-loaded superparamagnetic iron oxide nanoparticles with human serum albumin-a biophysical study', *J. Pharm. Innov.*, 2015, **10**, (1), pp. 13–20
[18] Kong J., Yu S.: 'Fourier transform infrared spectroscopic analysis of protein secondary structures', *Acta Bioch. Bioph. Sin.*, 2007, **39**, (8), pp. 549–559
[19] Hamdani S., Joly D., Carpentier R., *ET AL.*: 'The effect of methylamine on the solution structures of human and bovine serum albumins', *J. Mol. Struct.*, 2009, **936**, (1–3), pp. 80–86
[20] Würthner F., Chen Z., Hoeben F.J.M., *ET AL.*: 'Supramolecular p-n-heterojunctions by co-self-organization of oligo (p-phenylene vinylene) and perylene bisimide dyes', *J. Am. Chem. Soc.*, 2004, **126**, (34), pp. 10611–10618
[21] Bell T.W., Hext N.M.: 'Supramolecular optical chemosensors for organic analytes', *Chem. Soc. Rev.*, 2004, **33**, (9), pp. 589–598
[22] Shahabadi N., Khorshidi A., Moghadam N.H.: 'Study on the interaction of the epilepsy drug, zonisamide with human serum albumin (HSA) by spectroscopic and molecular docking techniques', *Spectrochim. Acta A*, 2013, **114**, pp. 627–632
[23] Wahba M.E.K., El-Enany N., Belal F.: 'Application of the Stern-Volmer equation for studying the spectrofluorimetric quenching reaction of eosin with clindamycin hydrochloride in its pure form and pharmaceutical preparations', *Anal. Methods – UK*, 2015, **7**, (24), pp. 10445–10451
[24] Meti M.D., Nandibewoor S.T., Chimatadar S.A.: 'Binding studies of lincosamide antibiotic drug clindamycin phosphate to human serum albumin by fluorescence, 3D, and circular dichroism spectroscopy', *Monatsh. Chem.*, 2014, **145**, (9), pp. 1519–1527
[25] Ware W.R.: 'Oxygen quenching of fluorescence in solution: an experimental study of the diffusion process', *J. Phys. Chem.*, 1962, **66**, (3), pp. 455–458
[26] Lakowicz J.R., Weber G.: 'Quenching of protein fluorescence by oxygen. Detection of structural fluctuations in proteins on the nanosecond time scale', *Biochemistry*, 1973, **12**, (21), pp. 4171–4179
[27] Hu Y.J., Liu Y., Wang J.B., *ET AL.*: 'Study of the interaction between monoammonium glycyrrhizinate and bovine serum albumin', *J. Pharmaceut. Biomed.*, 2004, **36**, (4), pp. 915–919
[28] Leckband D.: 'Measuring the forces that control protein interactions', *Annu. Rev. Bioph. Biom.*, 2000, **29**, (1), pp. 1–26
[29] Li J., Li J., Jiao Y., *ET AL.*: 'Spectroscopic analysis and molecular modeling on the interaction of jatrorrhizine with human serum albumin (HSA)', *Spectrochim. Acta A*, 2014, **118**, pp. 48–54
[30] Ross P.D., Subramanian S.: 'Thermodynamics of protein association reactions: forces contributing to stability', *Biochemistry*, 1981, **20**, (11), pp. 3096–3102
[31] Siamwiza M.N., Lord R.C., Chen M.C., *ET AL.*: 'Interpretation of the doublet at 850 and 830 cm^{-1} in the Raman spectra of tyrosyl residues in proteins and certain model compounds', *Biochemistry*, 1975, **14**, (22), pp. 4870–4876
[32] Choi S.M., Ma C.Y.: 'Structural characterization of globulin from common buckwheat (Fagopyrum esculentum moench) using circular dichroism and Raman spectroscopy', *Food Chem.*, 2007, **102**, (1), pp. 150–160
[33] Yu N.T., Jo B.H., O'shea D.C.: 'Laser Raman scattering of cobramine B, a basic protein from cobra venom', *Arch. Biochem. Biophys.*, 1973, **156**, (1), pp. 71–76
[34] Jurasekova Z., Marconi G., Sanchez-Cortes S., *ET AL.*: 'Spectroscopic and molecular modeling studies on the binding of the flavonoid luteolin and human serum albumin', *Biopolymers*, 2009, **91**, (11), pp. 917–927
[35] Aliaga A.E., Osorio-Román I., Leyton P., *ET AL.*: 'Surface-enhanced Raman scattering study of L-tryptophan', *J. Raman Spectrosc.*, 2009, **40**, (2), pp. 164–169

© The Institution of Engineering and Technology 2018

doi: 10.1049/mnl.2018.0165